光学学报

二苯并吡啶并喹喔啉类延迟荧光材料的合成及其电致发光性质

杨耀祖[1]，黄飞翔[1]，谢凤鸣[2]，张强[1]，袁国[1]，胡英元[1**]，赵鑫[1*]

[1]苏州科技大学化学与生命科学学院，江苏 苏州 215009；

[2]苏州大学功能纳米与软物质研究院江苏省碳基功能材料与器件重点实验室，江苏 苏州 215123

摘要 为获得新颖高效的热激活延迟荧光(TADF)材料，以二苯并吡啶并喹喔啉(BPQ)为受体(A)，三苯胺(TPA)、吩噁嗪(PXZ)为供体(D)，合成两种TADF材料：BPQPXZ和BPQTPA。研究表明，两种材料都具有典型的延迟荧光特性、较小的单重态与三重态的能级差(ΔE_{ST})和较大的振子强度(f)。基于强受体强供体组合的BPQPXZ的器件实现了深红光发射，发射波长达到660 nm，但受能隙的影响，外量子效率(EQE)仅有1.0%。基于强受体弱供体组合的BPQTPA，因其TPA刚性小于PXZ，BPQTPA的供受体扭曲程度小，轨道交盖程度大，f更大，故BPQTPA具有更大的荧光量子产率(82.7%)。同时因TPA的给电子能力比PXZ弱，BPQTPA内电荷转移效应减小，导致发射峰蓝移，因此基于BPQTPA的器件发射555 nm的黄光，与BPQPXZ相比，BPQTPA器件的启亮电压降低至2.8 V，电流效率、功率效率分别提高了32倍和36倍，EQE提升了6倍，达到7.0 %。

关键词 材料；延迟荧光；有机发光二极管；二苯并吡啶并喹喔啉；电致发光

中图分类号 O469 **文献标志码** A **DOI**：10.3788/AOS231985

1 引 言

有机发光二极管(OLED)因具有质量轻、灵活性强、响应快、色域宽等优点，在全彩色显示器和固态照明等领域受到了广泛关注[1-7]。发光材料作为OLED的核心，已经发展到第三代热活化延迟荧光(TADF)材料。相比于第二代重金属配合物磷光材料，TADF材料可以在实现100%理论内量子效率的同时避免使用重金属原子，解决了毒性大和环境污染等问题，更重要的是，TADF材料具有第一代传统荧光材料成本低廉的优点，因此其商业化应用前景十分广阔[8-9]。目前，基于TADF材料的OLED器件的外量子效率(EQE)已经达到40%左右[10-14]。但是，这些具有高EQE的TADF-OLED器件多数基于蓝光或者绿光材料，相比之下，橙光和红光TADF材料的发展仍然相对滞后。根据能隙定律，具有低发射态的红光TADF材料通常会发生严重的非辐射衰变，导致高效率的红光TADF材料还很稀缺。因此，开发高效的长波长TADF材料对于TADF-OLED的发展显得十分重要和迫切[15-19]。

目前，设计发光性能优异的供体-受体(D-A)型长波长TADF材料主要有两种途径：一是设计D-A大共轭平面结构来获得高单线态荧光辐射率。通过增大分子的最高占有分子轨道(HOMO)和最低未占分子轨道(LUMO)的重叠面积来加大最低单重激发态(S_1)和基态(S_0)之间的振子强度(f)，从而提高TADF材料的辐射转换率[20-21]。例如，赵祖金课题组[22]开发了一种红色的TADF材料DCPPr-α-NDPA，该材料的分子结构具有轻微扭曲的几何形状，有利于HOMO-LUMO重叠，其电致发光波长为606 nm，最大EQE为31.5%。二是设计高度扭曲的D-A结构，实现HOMO和LUMO的充分分离，从而得到小的单重态与三重态之间的能极差(ΔE_{ST})。较小的ΔE_{ST}有利于激子进行快速的反向系间窜越(RISC)，从而提高三重态(T_1)激子的利用率，进而实现TADF材料的高效发光[23-24]。例如，郑才俊课题组[13]合成了橙红光TADF材料SAF-2NP，高度扭曲的分子结构使该材料的HOMO和LUMO的交盖程度很小，从而得到较小的ΔE_{ST}(0.04 eV)和较高的RISC速率($1.91\times10^5\ s^{-1}$)，其掺杂器件的发射波长为576 nm，最大EQE为32.5%。可见，实现高荧光辐射率与获得小的ΔE_{ST}存在着不可避免的矛盾，实现二者的较好平衡具有重要意义。通常情况下，大的共轭结构有利于TADF材料发射波长红移，实现橙光和红光发射；刚性结构可以有效抑制

收稿日期：2023-12-25；**修回日期**：2024-01-30；**录用日期**：2024-02-05；**网络首发日期**：2024-02-20

基金项目：国家自然科学基金(21905048，52303244)、江苏省研究生研究创新项目(KYCX23_3342)

通信作者：*zhaoxinsz@usts.edu.cn；**741015344@qq.com

TADF分子的非辐射跃迁，有利于获得高的光致荧光量子产率（PLQY）值。近年来，Sun等[25]报道了一种新型红光TADF材料DBP-4MOTPA，该材料同时具有刚性骨架结构和大共轭平面分子结构，PLQY值达到65%，EQE值达到10.2%；本课题组[26]成功制备出橙红光TADF材料1PXZ-BP，其PLQY值达到73%，掺杂器件EQE达到26.3%；李成龙课题组[17]报道了一种TADF材料TPA-APQDCN-C，在610 nm处发射红色荧光，EQE达到34.3%；廖良生课题组[18]报道了一种红光TADF材料TPA-PZCN，在648 nm处发射深红色荧光，PLQY值高达97%，EQE达到28.1%；李涛课题组[19]报道了一系列基于同一受体吩嗪，连接不同供体，通过分析构效关系实现了从蓝光到红光的调控，为设计高性能、多色光的TADF材料提供了新的策略。

含氮类多环芳香烃具有深的LUMO，因此被当作受体单元并广泛用于合成长波长TADF材料。二苯并吡啶并喹喔啉（BPQ）分子中有5个稠合的共轭芳香环和3个sp^2杂化的N原子，其LUMO较深，达到−2.39 eV[27]，因此BPQ具有大的刚性共轭平面和强吸电子能力，是一种非常适合用来开发高效长波长TADF材料的受体。基于此，本文以BPQ为受体，给电子性能不同的三苯胺（TPA）和吩噁嗪（PXZ）为供体，采用易操作的Suzuki和Buchwald等偶联反应合成了两种D-A型TADF材料：BPQTPA和BPQPXZ。在核磁共振氢谱（^{1}H NMR）和高分辨质谱（HRMS）表征其结构的基础上，对两种材料的光物理性质、电化学性质和热性质及其构效关系进行详细研究，并分别以两种材料为发光层制备OLED器件，对它们的电致发光性能进行分析。

2 实验部分

2.1 实验试剂、仪器与方法

药品和催化剂等购于上海皓鸿生物医药科技有限公司，试剂购于安徽泽升科技股份有限公司。^{1}HNMR由AVANCE III 400 MHz核磁共振波谱仪（德国布鲁克公司）测定；质谱由Agilent qtof 6550高分辨质谱仪（美国安捷伦科技有限公司）测定；紫外吸收谱由TU-1901型紫外-可见分光光度计（北京普析通用仪器有限责任公司）测定；荧光光谱由LS55型荧光分光光度计（铂金埃尔默股份有限公司）测定；电化学测定由RST 3100型电化学工作站（苏州瑞思特仪器有限公司）测定；TGA由HCT-2型微机差热天平（北京恒久科学仪器厂）测定；低温磷光谱由FLS 920型光谱仪（英国爱丁堡仪器有限公司）测定。

中间体与目标产物均通过重结晶或柱色谱分离提纯，以氘代氯仿（$CDCl_3$）为溶剂测定核磁共振谱。将目标化合物配成浓度为10^{-5} mol·L^{-1}的甲苯溶液，测定紫外-可见光吸收光谱和荧光光谱；配制浓度为10^{-3} mol·L^{-1}的2-甲基四氢呋喃溶液，并在77 K下测定其荧光光谱和磷光光谱；用热重分析（TGA）法测试化合物的TGA曲线；将二茂铁作为内标，铂碳为工作电极，Ag/AgCl为参比，铂丝为辅助电极，四丁基高氯酸铵为电解质，测定目标分子的循环伏安曲线；以密度泛函理论（DFT）为基础，采用Gaussian 09软件的B3LYP法计算HOMO和LUMO分布，并结合6-31G机组模拟得到其轨道电子云分布。

2.2 合成与表征

BPQTPA和BPQPXZ的合成路线如图1所示。

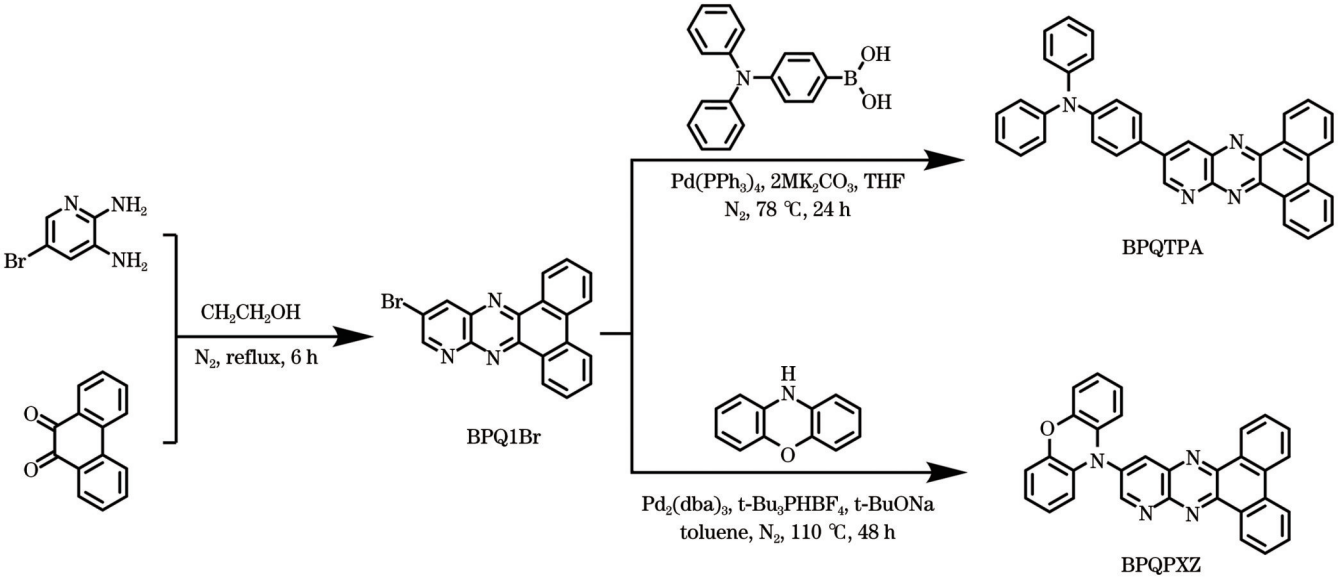

图1 BPQTPA和BPQPXZ的合成路线

Fig. 1 Synthetic routes of BPQTPA and BPQPXZ

1）4-(二苯并[f,h]吡啶并[2,3-b]喹喔啉-12-基)-*N*,*N*-二苯基苯胺(BPQTPA)的合成

在N_2环境下，将菲-9,10-二酮(0.70 g,3.36 mmol)和5-溴吡啶-2,3-二胺(0.69 g,3.70 mmol)溶于40 mL无水乙醇溶液中，溶液在85 ℃下搅拌回流6 h。中间产物12-溴二苯并[f,h]吡啶[2,3-b]喹啉(BPQ1Br)(0.95 g,2.64 mmol)通过真空抽滤分离。将BPQ1Br(0.95 g,2.64 mmol)、(4-(二苯胺)苯基)硼酸(0.91 g,3.26 mmol)和$Pd(PPh_3)_4$(质量分数为5%)置于三口瓶中，用N_2气体置换3次，加入40 mL四氢呋喃和10 mL浓度为2 mol/L的K_2CO_3溶液。溶液在N_2保护下回流搅拌24 h(@80 ℃)。反应结束后，将混合物倒入NaOH溶液中，搅拌后静置30 min，将固体抽滤出来，用20 mL蒸馏水洗涤滤饼3遍。选用DCM溶剂作为洗脱液，用硅胶柱色谱纯化分离出产物，得到橙红色固体(1.29 g，收率为73.3%)。橙红色固体的特性如下：熔点(m.p.)>300 ℃；^{1}H NMR (400 MHz, $CDCl_3$)测得的化学位移(δ)为8.73～8.59[多重峰(m)，2H]、8.48[双重峰(d)，耦合常数(J)=8.0 Hz，1H]、7.85 (d, J=2.5 Hz, 1H)、7.72～7.64 (m, 2H)、6.93[三重峰(t)，J=7.6 Hz, 2H]、6.86 (t, J=9.4 Hz, 4H)、6.48～6.38 (m, 4H)、6.33[单峰(s)，1H]、6.29 (d, J=5.8 Hz, 5H)、6.20 (t, J=7.3 Hz, 2H)；HRMS[电喷雾电离(ESI)，质荷比(m/z)]测得的$C_{37}H_{24}N_4$质子化分子离子峰$[M+H]^+$为525.2001(计算值)、525.5517(实验值)。

2）10-(二苯并[f,h]吡啶并[2,3-b]喹喔啉-12-基)-10H-苯噁嗪(BPQPXZ)的合成

将BPQ1Br(0.80 g，2.22 mmol)、吩噁嗪(PXZ)(0.49 g，2.66 mmol)、叔丁醇钠(0.85 g，8.88 mmol)、$Pd_2(dba)_3$(质量分数为5%)和t-Bu_3PHBF_4(质量分数为5%)置于三口瓶中，用N_2气体置换3次，倒入45 mL甲苯。在N_2保护下回流搅拌48 h。反应结束后将反应液倒入150 mL蒸馏水中，使用DCM溶剂萃取3次。将DCM作为洗脱液，以硅胶柱色谱纯化目标产物，得到深红色固体(0.42 g，收率为37.8%)。深红色固体的特性如下：m.p.>300 ℃；^{1}H NMR (400 MHz, $CDCl_3$)测得的δ为9.29 (d, J=9.2 Hz, 1H)、9.20 (d, J=2.6 Hz, 1H)、8.71 (s, 1H)、8.55 (d, J=8.1 Hz, 2H)、7.89～7.65 (m, 5H)、6.73[四重峰(dd)，J=22.1, 8.0 Hz, 5H]，6.65～6.52 (m, 3H)；HRMS (ESI, m/z)测得的$C_{31}H_{18}N_4O$ $[M+H]^+$为463.1841(计算值)、463.3207(实验值)。

3　结果与讨论

3.1　DFT计算

为探究两种材料的几何构型、能级和轨道分布，使用Gaussian 09软件在B3LYP/6-31G*基组下进行DFT和时间依赖的DFT(TD-DFT)计算，得到它们优化后的分子几何构型、S_1和T_1能级，以及HOMO和LUMO的能级与分布，如图2所示。在BPQPXZ中，

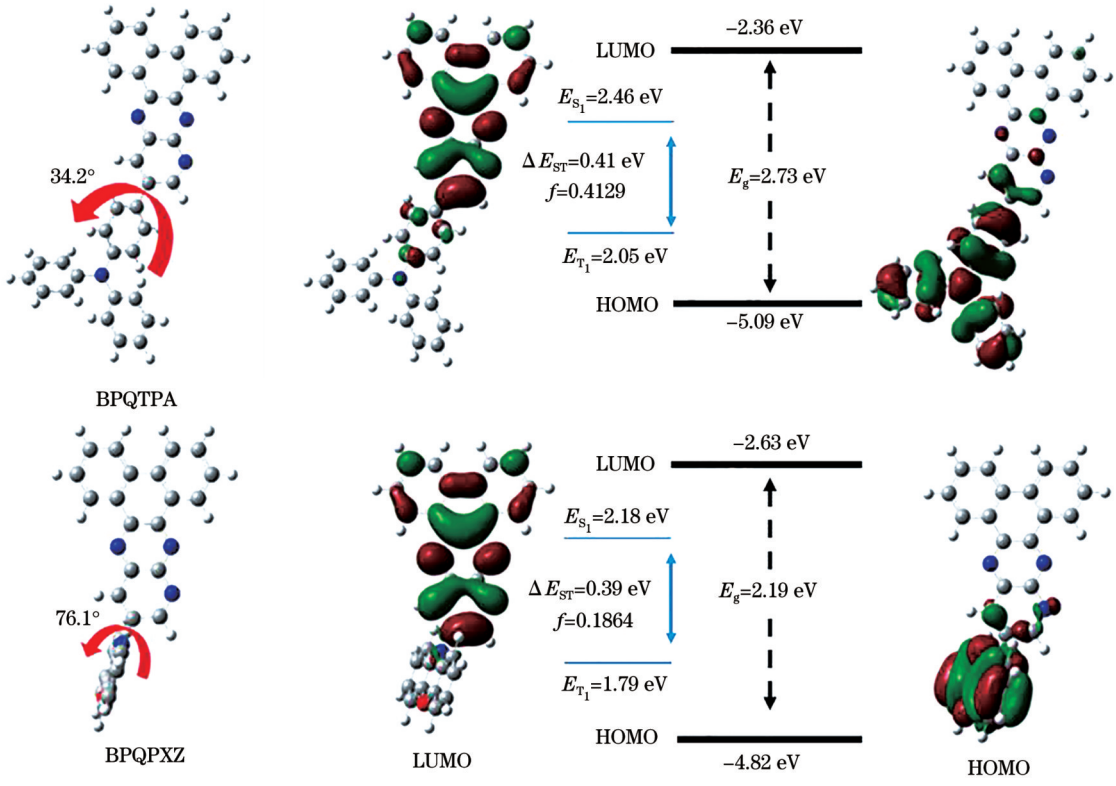

图2　BPQTPA和BPQPXZ的前沿分子轨道、能级和带隙

Fig. 2　FMOs, energy levels, and E_g of BPQTPA and BPQPXZ, respectively

刚性平面共轭受体BPQ与刚性供体PXZ之间的空间位阻较大，导致分子结构高度扭曲，二面角为76.1°，LUMO主要分布在受体BPQ上，而HOMO主要分布在供体PXZ上，并在受体上有轻微的延伸。结构的高度扭曲导致HOMO和LUMO的分离很好。此外，HOMO在受体有少量交盖，最终获得了小的ΔE_{ST}（0.39 eV）。BPQTPA的供体和受体之间的二面角只有34.2°，大幅降低的二面角归因于三苯胺（TPA）的刚性程度小于PXZ，导致分子趋于平面化，造成HOMO和LUMO的分离程度减小，交盖程度变大，结果使得ΔE_{ST}（0.41 eV）变大。供体的给电子能力越强，HOMO越浅。理论计算结果表明，BPQTPA和BPQPXZ的LUMO/HOMO能级分别为−2.36/−5.09 eV和−2.63/−4.82 eV。随着给电子能力的增强，HOMO与LUMO之间的带隙（E_g）逐渐减小，BPQTPA和BPQPXZ的E_g分别为2.73 eV和2.19 eV。同时，根据弗兰克-康登原理和费米黄金定则，HOMO和LUMO的交盖程度变大，导致辐射的振子强度（f）增大，从而提升材料的PLQY。BPQTPA的f高达0.4129，是BPQPXZ（f=0.1864）的2.2倍，可见，高的f有助于得到高的PLQY[28-30]。

3.2 光物理性质

为了分析BPQTPA和BPQPXZ的光物理性质，对两种材料进行了紫外-可见光（UV-vis）吸收光谱、低温荧光（LTFL）和低温磷光（LTPh）光谱的测试，结果如图3所示。在UV-vis吸收光谱中，BPQTPA在329 nm和388 nm处的吸收峰主要来自分子内的电子从π轨道到π*轨道（π-π*）和从n轨道到π*轨道（n-π*）跃迁，在457 nm附近的吸收峰主要归因于TPA供体到BPQ受体的分子内电荷转移（ICT）过程；BPQPXZ在302 nm、314 nm和379 nm、396 nm的吸收峰分别来自分子内的π-π*和n-π*跃迁，在519 nm处较宽的吸收峰来源于PXZ供体到BPQ受体的ICT过程。BPQTPA和BPQPXZ两种材料的紫外吸收带边（λ_{onset}）分别为521 nm和626 nm，根据公式E_g=1240/λ_{onset}[31-32]，计算得出它们的E_g分别为2.38 eV和1.98 eV。低温荧光光谱表明，BPQPXZ与BPQTPA的荧光发射波长分别为655 nm和585 nm，实现了红光和橙红光发射。TPA的给电子能力弱于PXZ，因此BPQTPA的ICT吸收带和光致发光（PL）光谱均明显蓝移，这和理论模拟计算的结果一致。根据低温荧光和低温磷光光谱计算得到BPQTPA和BPQPXZ的ΔE_{ST}分别为0.12 eV和0.07 eV，这是因为BPQTPA的供体和受体单元之间的扭转角较小，导致HOMO-LUMO的空间重叠更多，因此ΔE_{ST}较大，这也与理论计算结果的趋势相同。BPQTPA和BPQPXZ的ΔE_{ST}均较小，有利于发生有效的RISC而实现延迟荧光发射。以罗丹明B为参比物质，得到BPQTPA和BPQPXZ的相对PLQY值分别为82.7%和22.3%。BPQTPA具有较高的PLQY，与理论计算的高振子强度一致，这有助于材料实现较优的器件性能[29-30]。

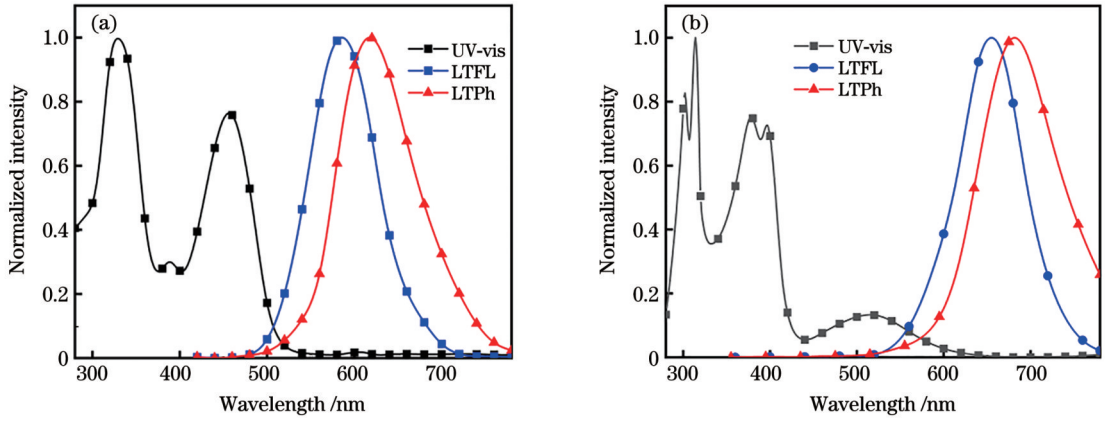

图3 BPQTPA和BPQPXZ紫外-可见光吸收光谱（室温）、低温荧光和磷光光谱（77 K）。(a) BPQTPA；(b) BPQPXZ

Fig. 3 Normalized UV-vis absorption at room temperature and fluorescence spectra and phosphorescence spectra at 77 K of BPQTPA and BPQPXZ, respectively. (a) BPQTPA; (b) BPQPXZ

为进一步研究其延迟荧光特性，分别掺杂质量分数为5%的BPQTPA和BPQPXZ到mCBP中制备薄膜，并在室温下测量其瞬态荧光衰减曲线，如图4所示。BPQTPA和BPQPXZ均显示出明显的双指数衰减特征，这是因为它们的荧光发射过程中既包含了从S_1到S_0的瞬时荧光衰减过程，又包含了从T_1到S_1再到S_0的延迟荧光衰减过程，是TADF化合物最典型的荧光发射特征[33]。测试结果表明，BPQTPA和BPQPXZ的瞬时荧光寿命（τ_p）和延迟荧光寿命（τ_d）分别为1.91 ns/0.08 μs和11.42 ns/0.21 μs，证明它们都具有延迟荧光（DF）性质，而τ_d时间较短则证明了分子的快速RISC过程。因此，BPQTPA和BPQPXZ具有TADF特性。

3.3 电化学性质

采用循环伏安（CV）法研究了BPQTPA和BPQPXZ的电化学性质，结果如图5所示。

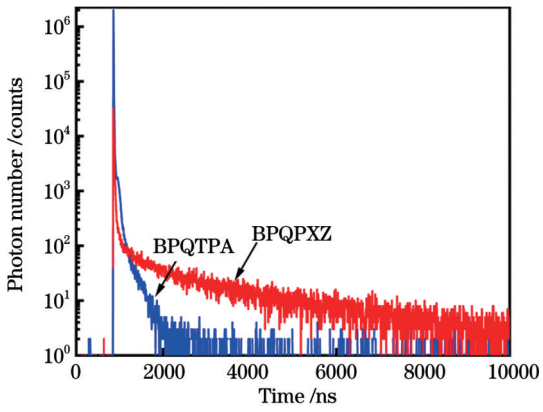

图 4　BPQTPA 和 BPQPXZ 在掺杂 mCBP 薄膜中的瞬态荧光衰减曲线

Fig. 4　Transient fluorescence decay curves of BPQTPA and BPQPXZ in doped mCBP films

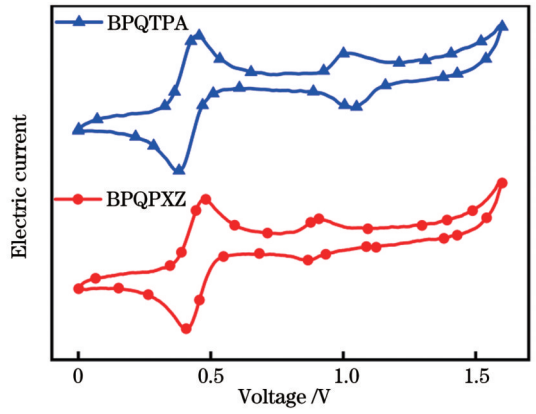

图 5　BPQTPA 和 BPQPXZ 的循环伏安曲线

Fig. 5　Cyclic voltammetry curves of BPQTPA and BPQPXZ

BPQTPA 和 BPQPXZ 都显示了可逆的氧化还原过程，表现出良好的电化学稳定性。使用二茂铁作为内标，根据氧化曲线的初始氧化电位和公式[34] $E_{HOMO}=-\left[E_{OX}-E_{1/2}\left(F_c/F_c^+\right)+4.8\ eV\right]$（$E_{HOMO}$ 为 HOMO 能级，E_{OX} 为起始氧化电势，$E_{1/2}(F_c/F_c^+)$ 为内标二茂铁的标准电势），可以计算出它们的 HOMO 能级分别为 −5.38 eV 和 −5.25 eV。根据公式 $E_{LUMO}=E_g+E_{HOMO}$，可以计算出它们相应的 LUMO 能级分别为 −3.00 eV 和 −3.27 eV。

3.4　热性质

用热重分析（TGA）法研究了 BPQTPA 和 BPQPXZ 的热性质（图 6）。当质量损失 5% 时，BPQTPA 和 BPQPXZ 的分解温度（T_d）分别为 492.6 ℃和 439.2 ℃，从两个化合物中都没有观察到明显的玻璃化转变，这应归因于它们的高刚性结构。上述结果表明两个 TADF 材料均具有良好的热稳定性，适合采用气相真空沉积法制备 OLED 器件，而它们的良好热性质也为 OLED 器件的稳定性提供了有力保障[35-36]。BPQTPA 和 BPQPXZ 的光物理性质、电化学性质和热性质的数据见表 1。

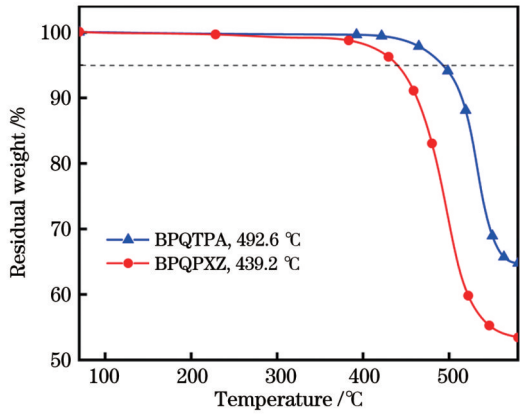

图 6　BPQTPA 和 BPQPXZ 的热重分析曲线

Fig. 6　Thermogravimetric analysis curves of BPQTPA and BPQPXZ

表 1　两种化合物的光物理、电化学和热性质的总结

Table 1　Summary of photophysical, electrochemical, and thermal properties of two compounds

Compound	λ_{abs} a) /nm	λ_{FL} a) /nm	λ_{Ph} a) /nm	E_{HOMO} b) /eV	E_{LUMO} c) /eV	E_g d) /eV	T_d e) /℃	PLQY f) /%	ΔE_{ST} g) /eV
BPQPXZ	302, 314, 379, 396, 519	655	681	−5.25	−3.27	1.98	439.2	22.3	0.07
BPQTPA	329, 388, 457	585	619	−5.38	−3.00	2.38	492.6	82.7	0.12

Notes: a) UV-vis absorption spectra at room temperature, fluorescence and phosphorescence spectra at 77 K measured; b) HOMO energy levels calculated from the initial oxidation potential; c) $E_{LUMO}=E_{HOMO}+E_g$; d) E_g values calculated by the onset of UV-vis absorption spectra; e) decomposition temperature (T_d) with 5% weight loss determined from TGA spectra; f) relative PLQY based on rhodamine B; g) ΔE_{ST} values estimated from the onset of the fluorescence and phosphorescence spectra.

3.5　OLED 器件的制备与性能

为了分析 BPQTPA 和 BPQPXZ 所制备器件的性能，利用这两种材料制备了多层 OLED 器件，器件结构为 ITO/HAT-CN(10 nm)/TAPC(60 nm)/TCTA(10 nm)/CBP：5% TADF (20 nm)/B3PYMPM(45 nm)/Liq(2 nm)/Al(100 nm)。阳极和阴极分别为 ITO 和 Al，空穴注入层和电子注入层分别为 HAT-CN 和 Liq，空穴传输层和电子传输层分别为 TAPC 和 B3PYMPM，能级和器件性能的结果如图 7 所示，主要的电致发光（EL）数据见表 2。

以 BPQPXZ 为发光层的掺杂 OLED 器件在 660 nm 处发射深红光，对应的国际照明委员会（CIE）

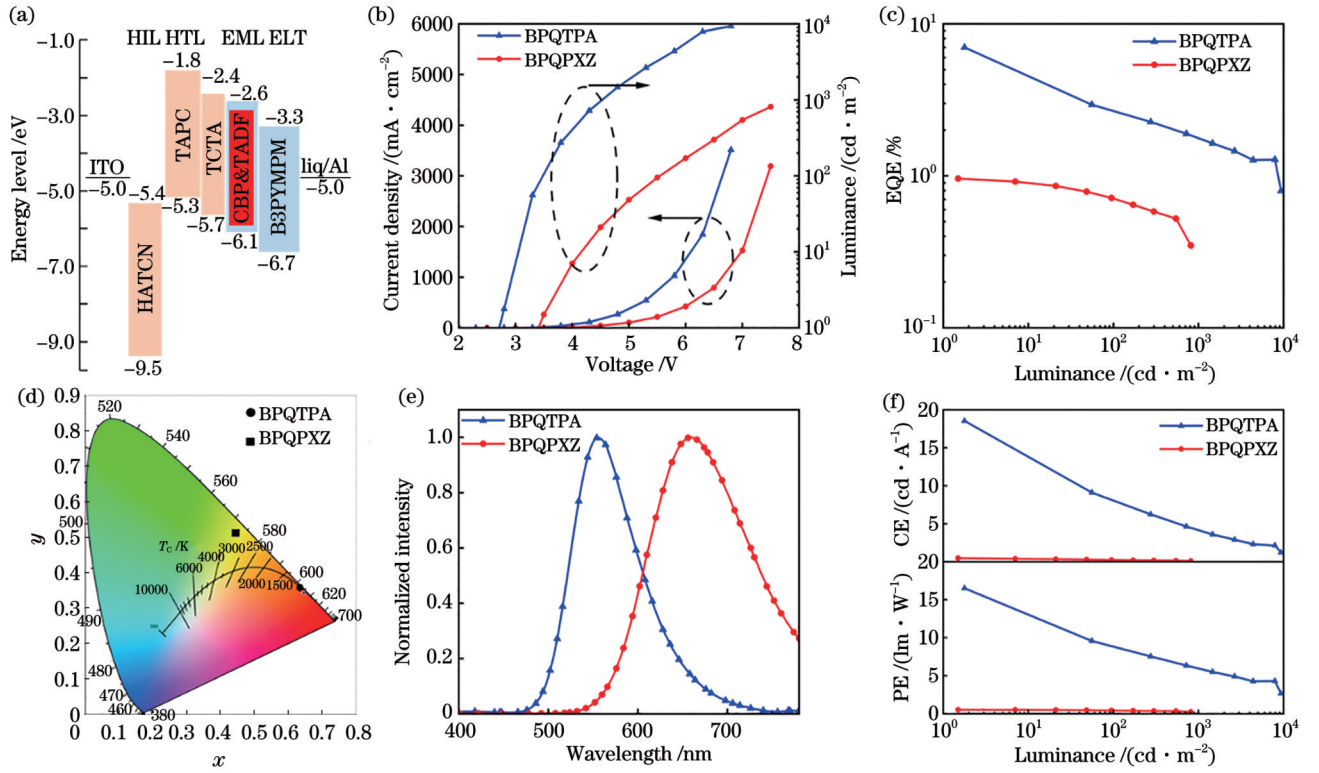

图 7　OLED 器件的能级结构和性能。(a)能级结构；(b)电流密度-电压-亮度特性曲线；(c)EQE 与亮度的关系曲线；(d)CIE 坐标；(e)EL 光谱；(f)CE 与亮度的关系曲线和 PE 与亮度的关系曲线

Fig. 7　Energy level structure and performance of OLED devices. (a) Energy level structure; (b) current density-voltage-luminance characteristic curves; (c) EQE versus luminance curves; (d) CIE coordinates; (e) EL spectra; (f) CE versus luminance curves and PE versus luminance curves

表 2　两种化合物器件性能的比较

Table 2　Comparison of device performance of two compounds

Compound	λ_{EL} [e)] /nm	V_{on} [a)] /V	EQE [b)] /%	PE [c)] /(lm•W^{-1})	CE [d)] /(cd•A^{-1})	CIE [f)] (x, y)
BPQPXZ	660	3.5	1.0	0.5	0.5	(0.65, 0.34)
BPQTPA	555	2.8	7.0	18.5	16.5	(0.45, 0.50)

Notes: a) turn-on voltage at 1 cd/m^2; b) maximum external quantum efficiency; c) maximum power efficiency; d) maximum current efficiency; e) EL emission peak; f) Commission Internationale del'Éclairage coordinates.

色坐标为(0.65, 0.34)，启亮电压(V_{on})为 3.5 V，最大电流效率(CE)为 0.5 cd/A，最大功率效率(PE)为 0.5 lm/W，但受能隙影响，非辐射衰减严重，EQE 仅为 1.0%。由于 TPA 的供电子能力弱于 PXZ，其 ICT 效应减弱，因此基于 BPQTPA 的器件发光波长蓝移，发射 555 nm 的黄光，对应的 CIE 色坐标为(0.45, 0.50)。与 BPQPXZ 相比，BPQTPA 的最大 CE、PE 和 EQE 均得到显著提升，CE、PE 分别提升到 16.5 cd/A 和 18.5 lm/W，EQE 提升到 7.0%，且器件 V_{on} 仅有 2.8 V，降低了 0.7 V。这是因为，根据 EQE(γ_{EQE})计算公式[37] $\gamma_{EQE}=\gamma_{IQE}\times\eta_{out}=\gamma\times\chi\times\varphi_{PL}\times\eta_{out}$($\gamma_{EQE}$ 为外量子效率，γ_{IQE} 为内量子效率，η_{out} 为光耦合输出效率，γ 为复合的载流子数与注入载流子数的比例，χ 为单线态激子百分数，φ_{PL} 为光致荧光量子产率)，与 BPQPXZ 相比，BPQTPA 具有更高的振子强度、更大的 PLQY(φ_{PL})值，因此其获得到相对更好的器件性能；还有可能与 BPQTPA 的轨道能级与器件中的空穴传输层和电子传输层的能级匹配性更好有关。

4　结　　论

以具有大刚性共轭平面的 BPQ 为受体，TPA、PXZ 为供体，设计合成了两种 TADF 材料：BPQTPA 和 BPQPXZ。研究发现，两种材料都具有典型的延迟荧光特性。两种 TADF 材料既实现了 HOMO 和 LUMO 较好的分离，也实现了一定程度的轨道重叠，因此获得了较小的 ΔE_{ST} 和较大的振子强度。基于强受体强供体组合的 BPQPXZ 的 OLED 器件，实现了深红光发射，发射波长达到 660 nm，但受能隙的影响，非辐射衰减严重，EQE 仅有 1.0%，电流效率、功率效率也不高。基于强受体弱供体组合的 BPQTPA，其

TPA刚性小于PXZ，使得BPQTPA的供受体扭曲程度小于BPQPXZ，其HOMO和LUMO的交盖程度增多，BPQTPA的振子强度为BPQPXZ的2.2倍，因此BPQTPA具有更大的PLQY（82.7%）。同时，供体TPA的给电子能力比PXZ弱，导致BPQTPA内电荷转移效应减弱，造成光致和电致发光峰均显著蓝移，因此基于BPQTPA的器件发射555 nm的黄光，与BPQPXZ器件相比，BPQTPA器件的启亮电压降低至2.8 V，电流效率、功率效率均获得显著提升，分别提高了32倍和36倍，EQE则提升了6倍，达到7.0%。本研究通过构效关系分析供受体合理组合对材料光物理性质和电致发光性质的影响，这对长波长TADF材料的研究具有一定的借鉴意义。

参 考 文 献

[1] Tang C W, VanSlyke S A. Organic electroluminescent diodes[J]. Applied Physics Letters, 1987, 51(12): 913-915.

[2] Kaltenbrunner M, Sekitani T, Reeder J, et al. An ultra-lightweight design for imperceptible plastic electronics[J]. Nature, 2013, 499(7459): 458-463.

[3] Fan X C, Hao X Y, Huang F, et al. RGB thermally activated delayed fluorescence emitters for organic light-emitting diodes toward realizing the BT. 2020 standard[J]. Advanced Science, 2023, 10(28): e2303504.

[4] Fan T, Zhu S, Cao X, et al. Tailored design of π-extended multi-resonance organoboron using indolo [3, 2-b] indole as a multi-nitrogen bridge[J]. Angewandte Chemie International Edition, 2023, 62(48): e202313254.

[5] 卢小香, 王勇, 韩晓媚, 等. 纳米图形增强OLED出光效率研究[J]. 激光与光电子学进展, 2018, 55(2): 022301.
Lu X X, Wang Y, Han X M, et al. Study on light extraction efficiency of enhanced OLED with nanopatterns[J]. Laser & Optoelectronics Progress, 2018, 55(2): 022301.

[6] 孙阿辉, 李耀召, 陈果, 等. 基于深蓝光激基复合物构筑的OLED植物照明光源[J]. 光学学报, 2022, 42(4): 0423001
Sun A H, Li Y Z, Chen G, et al. Organic light-emitting diodes based on deep-blue exciplex for plant growth[J]. Acta Optica Sinica, 2022, 42(4): 0423001.

[7] 潘赛虎, 于航, 赵云平, 等. 金属纳米颗粒的导入对顶发射OLED光取出影响的FDTD模拟与研究[J]. 光学学报, 2022, 42(9): 0916001.
Pan S H, Yu H, Zhao Y P, et al. FDTD simulation and study on effect of metal nanoparticle introduction on light extraction of top-emitting OLED[J]. Acta Optica Sinica, 2022, 42(9): 0916001.

[8] Uoyama H, Goushi K, Shizu K, et al. Highly efficient organic light-emitting diodes from delayed fluorescence[J]. Nature, 2012, 492(7428): 234-238.

[9] Sarada G, Cho W, Maheshwaran A, et al. Deep-blue phosphorescent Ir(III) complexes with light-harvesting functional moieties for efficient blue and white PhOLEDs in solution-process[J]. Advanced Functional Materials, 2017, 27(27): 1701002.

[10] Fu Y, Liu H, Tang B Z, et al. Realizing efficient blue and deep-blue delayed fluorescence materials with record-beating electroluminescence efficiencies of 43.4% [J]. Nature Communications, 2023, 14(1): 2019.

[11] Park D, Kang S, Ryoo C H, et al. High-performance blue OLED using multiresonance thermally activated delayed fluorescence host materials containing silicon atoms[J]. Nature Communications, 2023, 14(1): 5589.

[12] Cheng Y C, Fan X C, Huang F, et al. A highly twisted carbazole-fused DABNA derivative as an orange-red TADF emitter for OLEDs with nearly 40% EQE[J]. Angewandte Chemie: International Ed. in English, 2022, 61(47): e202212575.

[13] Zhang H Y, Yang H Y, Zhang M, et al. A novel orange-red thermally activated delayed fluorescence emitter with high molecular rigidity and planarity realizing 32.5% external quantum efficiency in organic light-emitting diodes[J]. Materials Horizons, 2022, 9(9): 2425-2432.

[14] Hu Y X, Miao J S, Hua T, et al. Efficient selenium-integrated TADF OLEDs with reduced roll-off[J]. Nature Photonics, 2022, 16: 803-810.

[15] Wang H, Chen J X, Shi Y Z, et al. An A-D-A-type thermally activated delayed fluorescence emitter with intrinsic yellow emission realizing record-high red/NIR OLEDs upon modulating intermolecular aggregations[J]. Advanced Materials, 2023: e2307725.

[16] Zeng W X, Lai H Y, Lee W K, et al. Achieving nearly 30% external quantum efficiency for orange-red organic light emitting diodes by employing thermally activated delayed fluorescence emitters composed of 1, 8-naphthalimide-acridine hybrids[J]. Advanced Materials, 2018, 30(5): 1704961.

[17] Yang T, Liang J X, Cui Y Y, et al. Achieving 34.3% external quantum efficiency for red thermally activated delayed fluorescence organic light-emitting diode by molecular isomer engineering[J]. Advanced Optical Materials, 2023, 11(1): 2201191.

[18] Zhang Y L, Ran Q, Wang Q, et al. High-efficiency red organic light-emitting diodes with external quantum efficiency close to 30% based on a novel thermally activated delayed fluorescence emitter[J]. Advanced Materials, 2019, 31(42): e1902368.

[19] Xie M C, Cai J H, Wang X Q, et al. Simple phenazine-based compounds realizing superior multicolored emission[J]. Advanced Optical Materials, 2022, 10(6): 2102443.

[20] Kumsampao J, Chaiwai C, Chasing P, et al. A simple and strong electron-deficient 5, 6-dicyano [2, 1, 3] benzothiadiazole-cored donor-acceptor-donor compound for efficient near infrared thermally activated delayed fluorescence[J]. Chemistry, 2020, 15(19): 3029-3036.

[21] Zhang Q S, Kuwabara H, Potscavage W J, Jr, et al. Anthraquinone-based intramolecular charge-transfer compounds: computational molecular design, thermally activated delayed fluorescence, and highly efficient red electroluminescence[J]. Journal of the American Chemical Society, 2014, 136(52): 18070-18081.

[22] Cai Z Y, Wu X, Liu H, et al. Realizing record-high electroluminescence efficiency of 31.5% for red thermally activated delayed fluorescence molecules[J]. Angewandte Chemie: International Ed. in English, 2021, 60(44): 23635-23640.

[23] Im Y, Kim M, Cho Y J, et al. Molecular design strategy of organic thermally activated delayed fluorescence emitters[J]. Chemistry of Materials, 2017, 29(5): 1946-1963.

[24] Mei Y, Liu D, Li J, et al. Acridin-9(10H)-one-based blue thermally activated delayed fluorescence materials: improvement of color purity and efficiency stability[J]. Materials Today Chemistry, 2022, 23: 100645.

[25] Sun K Y, Cai Z S, Jiang J F, et al. Multi-substituted dibenzo [a, c] phenazine derivatives as solution-processable thermally activated delayed fluorescence materials for orange-red organic light-emitting diodes[J]. Dyes and Pigments, 2020, 173: 107957.

[26] Xie F M, Wu P, Zou S J, et al. Efficient orange-red delayed fluorescence organic light-emitting diodes with external quantum efficiency over 26%[J]. Advanced Electronic Materials, 2020, 6(1): 1900843.

[27] Si C F, Hu Y N, Sun D M, et al. The influence of nitrogen

doping of the acceptor in orange-red thermally activated delayed fluorescence emitters and OLEDs[J]. Journal of Materials Chemistry C, 2023, 11(36): 12174-12184.
[28] Yang T, Cheng Z, Li Z Q, et al. Improving the efficiency of red thermally activated delayed fluorescence organic light-emitting diode by rational isomer engineering[J]. Advanced Functional Materials, 2020, 30(34): 2002681.
[29] Kim H S, Cheon H J, Lee D, et al. Toward highly efficient deep-blue OLEDs: tailoring the multiresonance-induced TADF molecules for suppressed excimer formation and near-unity horizontal dipole ratio[J]. Science Advances, 2023, 9(22): eadf1388.
[30] Meng G Y, Dai H Y, Wang Q, et al. High-efficiency and stable short-delayed fluorescence emitters with hybrid long- and short-range charge-transfer excitations[J]. Nature Communications, 2023, 14: 2394.
[31] Karuthedath S, Gorenflot J, Firdaus Y, et al. Intrinsic efficiency limits in low-bandgap non-fullerene acceptor organic solar cells [J]. Nature Materials, 2021, 20(3): 378-384.
[32] Wallace A M, Curiac C, Delcamp J H, et al. Accurate determination of the onset wavelength (λ_{onset}) in optical spectroscopy[J]. Journal of Quantitative Spectroscopy and Radiative Transfer, 2021, 265: 107544.
[33] Meng G Y, Zhou J P, Huang T Y, et al. B-N/B-O contained heterocycles as fusion locker in multi-resonance frameworks towards highly-efficient and stable ultra-narrowband emission[J]. Angewandte Chemie: International Ed. in English, 2023, 62(45): e202309923.
[34] Huo Y M, Lü J C, Xie Y C, et al. Structurally regulated carbazole-pyridine derivatives based on space-crowded theory for efficient narrowband ultraviolet nondoped organic light-emitting diodes from the high-lying reverse intersystem crossing process [J]. ACS Applied Materials & Interfaces, 2022, 14(51): 57092-57101.
[35] Liu T T, Yan Z P, Hu J J, et al. Chiral thermally activated delayed fluorescence emitters-based efficient circularly polarized organic light-emitting diodes featuring low efficiency roll-off[J]. ACS Applied Materials & Interfaces, 2021, 13(47): 56413-56419.
[36] Zhang Y P, Song S Q, Mao M X, et al. Efficient circularly polarized photoluminescence and electroluminescence of chiral spiro-skeleton based thermally activated delayed fluorescence molecules[J]. Science China Chemistry, 2022, 65(7): 1347-1355.
[37] Wu T L, Huang M J, Lin C C, et al. Diboron compound-based organic light-emitting diodes with high efficiency and reduced efficiency roll-off[J]. Nature Photonics, 2018, 12: 235-240.

Synthesis and Electroluminescence Properties of Delayed Fluorescence Materials Based on Dibenzopyridoquinoxaline

Yang Yaozu[1], Huang Feixiang[1], Xie Fengming[2], Zhang Qiang[1], Yuan Guo[1], Hu Yingyuan[1**], Zhao Xin[1*]

[1]*School of Chemistry and Life Sciences, Suzhou University of Science and Technology, Suzhou* 215009, *Jiangsu, China*;

[2]*Jiangsu Key Laboratory for Carbon-Based Functional Materials & Devices, Institute of Functional Nano & Soft Materials (FUNSOM), Soochow University, Suzhou* 215123, *Jiangsu, China*

Abstract

Objective To obtain novel and efficient thermally activated delayed fluorescence (TADF) materials, BPQPXZ and BPQTPA are synthesized using dibenzopyridoquinoxaline (BPQ) as acceptor (A) and triphenylamine (TPA) and phenoxazine (PXZ) as donors (D). The results show that the two materials have typical delayed fluorescence characteristics, a smaller energy gap (ΔE_{ST}) between singlet and triplet states, and a larger oscillator strength (f). The device based on BPQPXZ combined with a strong acceptor and a strong donor achieves deep-red emission with λ_{EL} at 660 nm. However, due to the influence of the energy-gap law, the external quantum efficiency (EQE) is only 1.0%. BPQTPA combined with a strong acceptor and a weak donor has a larger fluorescence quantum yield (82.7%) because of the weaker rigidity of TPA than that of PXZ. As a result, the donor and acceptor of BPQTPA have less distortion, more orbital overlap, and larger f. At the same time, the intramolecular charge transfer effect of BPQTPA is weakened, and the electron-donating ability of TPA is weaker than that of PXZ. BPQTPA exhibits a blue-shifted emission compared with BPQPXZ. Therefore, the device based on BPQTPA exhibits yellow emission with λ_{EL} at 555 nm. Compared with BPQPXZ, the turn-on voltage of BPQTPA is reduced to 2.8 V; the maximum current efficiency and power efficiency are increased by 32-fold and 36-fold, respectively, and the EQE is increased by 6-fold to 7.0%.

Methods In this study, BPQPXZ and BPQTPA materials are synthesized using the Suzuki reaction and Buchwald-Hartwig reaction. The photophysical properties, electrochemical properties, thermal properties, and device performance of the two materials are investigated. Comparative analysis is conducted on the luminescent properties of two materials.

Results and Discussions The structures of two materials, BPQPXZ and BPQTPA, are verified by ^{1}H nuclear magnetic

resonance (^{1}H NMR) spectroscopy and high-resolution mass spectrometry (HRMS). BPQPXZ exhibits deep-red emission with λ_{PL} at 655 nm, and BPQTPA exhibits yellow emission with λ_{PL} at 585 nm (Fig. 3). Compared with BPQPXZ, BPQTPA exhibits blue-shifted emission because of weaker electron-donating ability of TPA than PXZ. Similarly, the rigidity of TPA is weaker than that of PXZ, resulting in a greater degree of overlap between the HOMO and LUMO of BPQTPA, a higher oscillator strength, and a larger fluorescence quantum yield (82.7%) for BPQTPA, which is consistent with the density functional theory simulation results (Fig. 2). As shown in the transient PL decay spectra (Fig. 4), the delay component is observed, and such phenomena are typical behaviors of TADF. As shown in the cyclic voltammogram (Fig. 5), the HOMO levels of BPQTPA and BPQPXZ are −5.38 eV and −5.25 eV, respectively. The calculated LUMO levels are −3.00 eV and −3.27 eV for BPQTPA and BPQPXZ, respectively. BPQTPA shows better thermal stability with a higher decomposition temperature (T_d, with 5% weight loss) of 492.6 ℃ than BPQPXZ (T_d= 439.2 ℃). The higher thermal stability of BPQTPA can be ascribed to its better planarity than that of BPQPXZ. These devices based on BPQTPA and BPQPXZ achieve good performance (Fig. 7). The device based on BPQTPA exhibits much higher EQE (7.0%) than the device based on BPQPXZ (EQE is 1.0%), especially.

Conclusions In this study, BPQTPA and BPQPXZ materials are designed and synthesized using BPQ with a highly rigid conjugated planar structure as an acceptor and TPA and PXZ as donors. The results show that two materials have typical delayed fluorescence characteristics. BPQTPA and BPQPXZ achieve good orbital separation between HOMO and LUMO, as well as a certain degree of orbital overlap, resulting in a smaller ΔE_{ST} and a larger oscillator strength. The device based on BPQPXZ combined with a strong acceptor and a strong donor achieves deep-red emission with λ_{EL} at 660 nm. However, due to the influence of energy-gap law, non-radiative decay is serious, with an EQE of only 1.0%, as well as low current and power efficiency. The device based on BPQTPA combined with a strong acceptor and a weak donor is less rigid than that based on BPQPXZ, making the degree of donor and acceptor distortion of BPQTPA less than BPQPXZ, and the degree of overlap between HOMO and LUMO orbitals of BPQTPA increases, so oscillator strength of BPQTPA is 2.2 times that of BPQPXZ. As a result, BPQTPA has a higher PLQY (82.7%). Meanwhile, due to the much weaker electron-donating ability of TPA than PXZ, the intramolecular charge transfer effect of BPQTPA is weakened, resulting in a significant blue-shift in both photoluminescence and electroluminescence peaks. The device based on BPQTPA exhibits yellow emission with λ_{EL} at 555 nm. Compared with BPQPXZ, the turn-on voltage of the device based on BPQTPA is reduced to 2.8 V, and the current efficiency and power efficiency are significantly improved by 32-fold and 36-fold, respectively. The EQE is increased by 6-fold to 7.0%. In particular, we investigate the effects of reasonable combinations of donor and acceptor on the photophysical and electroluminescent properties of materials through structure-activity relationships, and the study is of certain reference significance for the research on long-wavelength TADF materials.

Key words materials; delayed fluorescence; organic light-emitting diodes; dibenzopyridoquinoxaline; electroluminescence